Published in final edited form as:
Inorg Chem. 2009 October 5; 48(19): 9316–9324. doi:10.1021/ic901161z.

Aryl bridged 1-Hydroxypyridin-2-one: Effect of the bridge on the Eu(III) sensitization process

Anthony D'Aléo, **Evan G. Moore**, **Géza Szigethy**, **Jide Xu**, and **Kenneth N. Raymond**
Chemical Sciences Division, Lawrence Berkeley National Laboratories, Berkeley, California 94720, and Department of Chemistry, University of California, Berkeley, California 94720-1460

Kenneth N. Raymond: raymond@socrates.berkeley.edu

Abstract

The efficiency of Eu3+ luminescence by energy transfer from an antenna ligand can be strongly dependent on the metal ion coordination geometry. The geometric component of the Eu(III) sensitization has been probed using series of tetradentate 1,2-HOPO derivatives that are connected by bridges of varying length and geometry. The ligands are N,N'-(1,2-phenylene)bis(1-hydroxy-6-oxo-1,6-dihydropyridine-2-carboxamide) for the ligand (L^1), 1-hydroxy-N-(2-(1-hydroxy-6-oxo-1,6-dihydropyridine-2-carboxamido)benzyl)-6-oxo-1,6-dihydropyridine-2-carboxamide (L^2) and N,N'-(1,2-phenylenebis(methylene))bis(1-hydroxy-6-oxo-1,6-dihydropyridine-2-carboxamide) (L^3). Spectroscopic characterization of both the Gd(III) and Eu(III) metal complexes, TD-DFT analysis of model compounds and evaluation of the kinetic parameters for the europium emission were completed. Some striking differences were observed in the luminescence quantum yield by altering the bridging unit. The $[Eu(L^2)_2]^-$ derivative shows efficient sensitization coupled with good metal centered emission. For $[Eu(L^3)_2]^-$, the large quenching of the luminescence quantum yield compared to $[Eu(L^2)_2]^-$ is primarily a result of one inner sphere water molecule bound to the europium cation while for $[Eu(L^1)_2]^-$, the low luminescence quantum yield can be attributed to inefficient sensitization of the europium ion.

Keywords

europium; gadolinium; luminescence; sensitization

Introduction

Luminescent lanthanide complexes have attracted much recent attention because of their use in a wide variety of applications such as bio-fluoroimmunoassay,[1, 2] as sensors,[3-7] in light emitting diodes,[8-10] and as waveguide amplifiers for lasers.[11-18] In most cases, these complexes consist of a lanthanide ion attached to a chelating chromophore which acts as a sensitizer, transferring its excitation energy to the lanthanide ion and protecting the ion from water coordination. The presence of the chromophore overcomes the limitation of an intrinsically small molar absorption coefficient (ε) for the metal by using a strongly absorbing organic ligand (*antenna effect*) by thus increasing the brightness (defined as the product of the luminescence quantum yield and of the molar absorption coefficient). The luminescence lifetimes of the lanthanide ions, which are highly sensitive to the local environment and especially to quenching by OH vibrations are maintained by keeping water molecules' out of the inner coordination sphere. The unique properties of these ions include

Correspondence to: Kenneth N. Raymond, raymond@socrates.berkeley.edu.

This technology is licensed to Lumiphore, Inc. in which some of the authors have a financial interest.

line like emission (going from the visible to the Near Infra-Red [NIR] by changing the lanthanide used), very long lifetimes (from the ms or sub-ms range for the visible emitters to the μs or sub-μs range for the NIR emitters) and the relative insensitivity of their emission to the presence of dioxygen.[19, 20]

Despite extensive research, the optimization of the energy transfer for the sensitization of the lanthanide ion by exciting complexed chromophores is still not fully understood. In this regard, the europium ion is an interesting probe since Beeby *et al*.[21] and Verhoeven *et al*.[22] have shown that the steady state luminescence spectrum and the luminescence lifetime of the europium ion can be used to evaluate the efficiency of the sensitization process.

Herein, we report the synthesis and optical studies of some aryl bridged 1-hydroxypyridin-2-one (1,2-HOPO) derivatives. The use of an aryl unit as a bridge[23] (compared to aliphatic versions previously published[24, 25]) has been shown recently to not significantly affect the triplet excited state energy, but has a strong effect on the luminescence quantum yield ranging from *ca*. 21% for aliphatic bridged derivatives to 6% for $\mathbf{[Eu(L^1)_2]^-}$ in aqueous solution at pH = 7.4. Furthermore, these types of 1,2-HOPO containing ligands have been previously shown to be efficient europium sensitizers and form highly stable complexes.[24, 25] In particular, the high thermodynamic stability of the complexes in aqueous solution allows measurements at μM and even nM concentrations without evidence of hydrolysis or dissociation. Following these observations, we have prepared two additional 1,2-HOPO derivatives containing a phenyl with one ($\mathbf{L^2}$) or two ($\mathbf{L^3}$) methylene group(s) in the ortho positions to isolate the phenyl group from one or both 1,2-HOPO units (Chart 1) and compared these systems to the already reported $\mathbf{[Eu(L^1)_2]^-}$ complex.[23] In order to better understand the differences between these systems, the photophysical data were analyzed using the methods described by Beeby[21] and Verhoeven[22] in three different solvents; two protic solvents (buffered water at pH = 7.4 and methanol) and an aprotic solvent (dimethylsulfoxide, DMSO).

Experimental

General

2-aminobenzylamine was purchased from Sigma-Aldrich while *α,α'*-diamino-*o*-xylene was synthetized as described elsewhere[26] as were L^1 and L^4 and their Gd and Eu complexes.[23,24, 25] Thin-layer chromatography (TLC) was performed using precoated Kieselgel 60 F254 plates. Flash chromatography was performed using EM Science Silica Gel 60 (230- 400 mesh). NMR spectra were obtained using either Bruker AM-300 or DRX-500 spectrometers operating at 300 (75) MHz and 500 (125) MHz for ^{1}H (or ^{13}C) respectively. ^{1}H (or ^{13}C) chemical shifts are reported in ppm relative to the solvent resonances, taken as δ 7.26 (δ 77.0) and δ 2.49 (δ 39.5) respectively for $CDCl_3$ and $(CD_3)_2SO$ (DMSO-d_6) while coupling constants (*J*) are reported in Hz. The following standard abbreviations are used for characterization of ^{1}H NMR signals: s = singlet, d = doublet, t = triplet, m = multiplet, dd = doublet of doublets. Fast-atom bombardment mass spectra (FAB^+ MS) were obtained using 3-nitrobenzyl alcohol (NBA) or thioglycerol/ glycerol (TG/G) as the matrix. Elemental analyses were performed by the Microanalytical Laboratory, University of California, Berkeley, CA.

Synthesis

General method for the preparation of Benzyl protected 1,2-HOPOBn derivatives—Over a one hour period, a solution of 1,2-HOPOBn acid chloride[27] (2.4 Eq) in dry dichloromethane (35 mL) was added dropwise to a mixture of the appropriate diamine derivative (1 Eq) and 30% potassium carbonate solution (5 mL) in dichloromethane (20 mL)

with vigorous stirring and external cooling by means of an ice bath. The mixtures were warmed to room temperature with stirring, until TLC indicated the reactions were complete. The organic phase was separated and the crude products were loaded on a flash silica column. Elution with 2-4% methanol in dichloromethane allowed for facile separation of the benzyl-protected precursors, which were all pale yellow oils that solidify upon standing.

2-Aminomethylaniline-1,2-HOPOBn ((L^{2}Bn))

Yield: 85%; ^{1}H NMR (500 MHz, $CDCl_3$): δ 4.32 (d, 2H), 4.79 (s, 2H), 5.37 (s, 2H), 6.33 (dd, ^3J = 7.0Hz, ^4J = 1.5Hz, 1H), 6.40 (m, 2H), 6.69 (dd, ^3J = 9.0Hz, ^4J = 1.5Hz, 1H), 6.84 (d, ^3J = 7.0Hz, 2H), 7.08 (m, 3H), 7.19-7.31 (m, 6H), 7.38 (d, ^3J = 7.5Hz, 1H), 7.44 (m, 3H), 8.01 (d, ^3J = 8.0Hz, 1H), 8.26 (s, 1H), 10.29 (s, 1H); ^{13}C NMR (125 MHz, $CDCl_3$): δ 39.7, 78.3, 78.8, 104.7, 106.4, 122.7, 123.0, 124.2, 125.9, 127.9, 128.3, 128.6, 129.3, 129.6, 129.8, 130.8, 132.1, 132.9, 134.5, 137.7, 137.8, 141.3, 143.0, 157.9, 158.1, 158.9, 160.4; FAB$^+$ MS: m/z: 577 (MH^+) (calc: 913.07).

o-Aminomethyl-benzylamine-1,2-HOPOBn ((L^{3}Bn))

Yield: 83%; ^{1}H NMR (500 MHz, $CDCl_3$): δ 4.44 (d, ^3J = 5.7 Hz, 4H), 5.08 (s, 4H), 6.19 (m, 4H), 7.04 (m, 2H), 7.10-7.15 (m, 2H), 720-7.40 (m, 12H), 7. 83 (m, 2H); ^{13}C NMR (125 MHz, $CDCl_3$): δ 40.5, 78.5, 105.3, 122.5, 127.8, 128.0, 128.7, 129.4, 132.8, 135.0, 142.5, 158.0, 159.9; FAB$^+$ MS: m/z: 590.6 ([M+H$^+$]) (calc: 590.6).

General method for the preparation of 1,2-HOPO derivatives—The appropriate 1,2-HOPOBn derivatives were dissolved in concentrated HCl (12 M)/glacial acetic acid (1:1, 20 mL), and were stirred at room temperature for 2 days. Filtration followed by removal of the solvent yielded residues, which were washed with ether to give the deprotected 1,2-HOPO ligands as off-white solids.

2-Aminomethylaniline-1,2-HOPO (L^2)

Yield: 86%; ^{1}H NMR (500 MHz, $CDCl_3$): δ 4.49 (s, 2H), 6.36 (d, ^3J = 7.0Hz, 1H), 6.58 (t, ^3J = 7.5Hz, 2H), 6.66 (d, ^3J = 9.0Hz, 1H), 7.26 (t, ^3J = 7.5Hz, 1H), 7.32 (t, ^3J = 7.5Hz, 3H), 7.39-7.52 (m, 4H), 9.28 (t, ^3J = 6.0 Hz, 1H), 10.62 (s, 1H); ^{13}C NMR (125 MHz, $CDCl_3$): δ 104.0, 104.5, 119.7, 125.5, 126.4, 127.5, 127.7, 132.6, 134.2, 137.2, 142.1, 157.5, 157.6, 159.2, 160.8; FAB$^+$ MS: m/z: 397.4 ([M+H$^+$]) (calc: 397.4); Anal calc (Found) for $C_{19}H_{16}N_4O_6$: C, 57.58(57.29); H, 4.07(4.01); N, 14.14(13.82).

o-Aminomethyl-benzylamine-1,2-HOPO (L^3)

Yield: 90%; ^{1}H NMR (500 MHz, DMSO-d_6): δ 4.50 (d, ^3J = 6.0 Hz, 4H), 6.35 (dd, ^3J = 7.0 Hz, ^4J= 1.5 Hz, 2H), 6.58 (dd, ^3J = 9.0 Hz, ^4J = 1.5 Hz, 2H), 7.26 (dd, ^3J = 5.5 Hz, ^4J = 2.1 Hz, 2H), 7.38 (m,4H), 9.26 (t, ^3J = 6.0 Hz, 2H); ^{13}C NMR (125 MHz, DMSO-d_6): δ 103.9, 119.6, 127.3, 127.9, 135.9, 137.4, 142.3, 157.6, 160.5; FAB$^+$ MS: m/z: 410.4 ([M+H$^+$]) (calc: 410.4); Anal calc (Found) for $C_{19}H_{16}N_4O_6$·MeOH: C, 57.02 (57.01); H, 4.59(5.01); N, 12.88(12.66).

General procedure for the preparation of lanthanide complexes—In a 25mL round bottom flask, the appropriate 1,2-HOPO derivative (2 Eq) was suspended in 2mL of methanol. Gadolinium(III) chloride hexahydrate or europium(III) chloride hexahydrate (1.02 Eq) in 3mL of methanol and two drops of pyridine were added. The solutions were heated to reflux for 4 h, then cooled to room temperature. Slow evaporation of the methanol at room temperature overnight afforded the desired complexes, as their pyridinium salts, which were collected by filtration.

Pyridinium[Gd(L^2)$_2$]

Yield: 30% (white solid); Anal calc (Found) for $C_{43}H_{34}N_9O_{12}Gd{\cdot}4H_2O$: C: 47.03(46.98), H: 3.86(3.73), N: 11.48(11.35); Found: C:, H:, N:; ESI-MS: [(GdL^2_2)$^-$]: m/z: 946.1 (calc: 946.1).

Pyridinium[Eu(L^2)$_2$]

Yield: 35% (white solid); Anal calc (Found) for $C_{43}H_{34}N_9O_{12}Eu{\cdot}4H_2O$: C: 47.26, H: 3.87, N: 11.54; Found: C: 47.37(47.26), H: 3.95(3.87), N: 11.41(11.54); ESI-MS: [(EuL^2_2)$^-$]: m/z: 941.2 (calc: 941.10).

Pyridinium[Gd(L^3)$_2$]

Yield: 43% (white solid); Anal calc (Found) for $C_{45}H_{38}N_9O_{12}Gd{\cdot}7H_2O$: C: 45.80(46.17), H: 4.44(3.94), N: 10.68(10.49); ESI-MS: [(GdL^3_2)$^-$]: m/z: 974.1 (calc: 974.14).

Pyridinium[Eu(L^3)$_2$]

Yield: 60% (white solid); Anal calc (Found) for $C_{45}H_{38}N_9O_{12}Eu{\cdot}4H_2O$: C: 48.22(48.36), H: 4.14(3.84), N: 11.25(11.11); Found: C:, H:, N:; ESI-MS: [(EuL^3_2)$^-$]: m/z: 969.2 (calc: 969.14).

Computational Studies

Ground state density functional theory (DFT) and time-dependent DFT (TD-DFT) calculations were performed at the Molecular Graphics and Computational Facility, College of Chemistry, University of California, Berkeley. In both cases, the B3LYP/6-311G++ (d,p) basis set provided in Gaussian'03[28] was used, with simplified input structures derived from a previously reported crystal structure[24, 25] All calculations were done in the gas phase and geometry optimizations were performed with no symmetry restraints. As a simplified model, only the 6-phenyl amide and 6-benzyl amide of 1,2-HOPO were used as the input structures, and these were first geometry optimized with no symmetry constraints to give the relaxed output geometries.

Optical spectroscopy

UV-Visible absorption spectra were recorded on a Varian Cary 300 double beam absorption spectrometer. Emission spectra were acquired on a HORIBA Jobin Yvon IBH FluoroLog-3 spectrofluorimeter, equipped with 3 slit double grating excitation and emission monochromators (2.1 nm/mm dispersion, 1200 grooves/mm). Spectra were reference corrected for both the excitation light source variation (lamp and grating) and the emission spectral response (detector and grating). Luminescence lifetimes were determined on a HORIBA Jobin Yvon IBH FluoroLog-3 spectrofluorimeter, adapted for time-correlated single photon counting (TCSPC) and multichannel scaling (MCS) measurements. A sub-microsecond Xenon flashlamp (Jobin Yvon, 5000XeF) was used as the lightsource, with an input pulse energy (100 nF discharge capacitance) of *ca*. 50 mJ, yielding an optical pulse duration of less than 300 ns at FWHM. Spectral selection was achieved by passage through the same double grating excitation monochromator. Emission was monitored perpendicular to the excitation pulse, again with spectral selection achieved by passage through the double grating emission monochromator (2.1 nm/mm dispersion, 1200 grooves/mm). A thermoelectrically cooled single photon detection module (HORIBA Jobin Yvon IBH, TBX-04-D) incorporating fast rise time PMT, wide bandwidth preamplifier and picosecond constant fraction discriminator was used as the detector. Signals were acquired using an IBH DataStation Hub photon counting module and data analysis was performed using the commercially available DAS 6 decay analysis software package from HORIBA Jobin Yvon IBH. Goodness of fit was assessed by minimizing the reduced chi squared function, χ^2, and

a visual inspection of the weighted residuals. Each trace contained at least 10,000 points and the reported lifetime values resulted from at least three independent measurements. Typical sample concentrations for both absorption and fluorescence measurements were *ca*. 10^{-5}-10^{-6} M and 1.0 cm cells in quartz suprasil or equivalent were used for all measurements. Quantum yields were determined by the optically dilute method (with optical density <0.1) using the following equation;

$$\Phi x/\Phi r=[Ar(\lambda r)/Ax(\lambda x)][I(\lambda r)/I(\lambda x)][nx2/nr2][Dx/Dr]$$

where *A* is the absorbance at the excitation wavelength (λ), *I* is the intensity of the excitation light at the same wavelength, *n* is the refractive index and *D* is the integrated luminescence intensity. The subscripts '*x*' and '*r*' refer to the sample and reference respectively. For quantum yield calculations, an excitation wavelength of 340 nm was utilized for both the reference and sample, hence the *I(λr)/I(λx)* term is removed. Similarly, the ratio of the refractive indices term, *nx2/nr2*, was assumed identical for the aqueous reference and sample solutions. Thus, a plot of integrated emission intensity (*i.e. Dr*) *vs*. absorbance at 340 nm (*i.e. Ar(λr)*) should be linear plot with a slope equal to the reference quantum yield Φ_r. Quinine sulfate in 0.5 M (1.0 *N*) sulfuric acid was used as the reference (Φ_r = 0.546). A plot of integrated emission intensity for the sample (*i.e. Dx*) versus absorbance at 340 nm gave the values reported, which are the average of four independent measurements.

Results and discussion

1. Synthesis

Each of the ligands investigated (Chart 1) incorporates the 1-hydroxypyridin-2-one (1,2-HOPO) group, which acts as a bidentate ligand to complex Ln(III) ions efficiently. The overall tetradentate ligand topology has been shown to form stable ML_2 complexes (where each ligand, L, is a bis-bidentate ligand composed of two such 1,2-HOPO chelates). These units can be linked by aliphatic[24, 25] or aromatic spacers[23] (Chart 1) *via* the amide functional groups. The benzyl protected 1,2-HOPO chromophore (Figure 1) was prepared as reported elsewhere.[29] The acid chloride was prepared *in situ* by using thionyl chloride[27] and the resulting intermediate (2.4 Eq) was combined with one equivalent of the corresponding diamine to furnish the benzyl protected tetradentate ligands. These were boiled in HCl and acetic acid to give the desired ligands in good yields. The Ln(III) complexes (Ln = Eu, Gd) were prepared by heating at reflux two equivalents of the appropriate ligand with one equivalent of $LnCl_3{\cdot}6H_2O$ using pyridine as a base. The product complexes were then precipitated and washed with ether to yield the pure hydrated complexes. X-ray quality crystals of $\mathbf{[Eu(L^1)_2]^-}$ and $\mathbf{[Eu(L^3)_2]^-}$ complex were grown by vapor diffusion of ether into methanol solutions (see ref 23 and supporting information, respectively).

2. Theoretical calculations

In order to obtain a more complete picture of the ligand ground and excited states, time-Dependent Density functional theory (DFT) calculations using the B3LYP functional were performed using Gaussian'03 following the method of Picard *et al*.,[30] The trivalent Ln cation was substituted by a monovalent Na atom. For $\mathbf{L^1}$ and $\mathbf{L^3}$ fragments, the resulting optimized geometry and relevant molecular orbital diagrams are depicted in Figure 2, and the resulting predicted electronic transitions in the UV/Vis region from TD-DFT analysis summarized in Table 1.

Details of the singlet and triplet state energies can be obtained from these calculations. The $\mathbf{L^1}$ and $\mathbf{L^3}$ linkages are well described by the model presented in Figure 2; the $\mathbf{L^2}$ linkage, with both a phenyl and benzyl linking unit, can be considered as a mixture of both $\mathbf{L^1}$ and

L^3. As noted elsewhere,[25] the calculated LUMO molecular orbital is metal centered, and transitions involving this orbital (*i.e*. involving an LMCT to the Na cation) is an artifact of the under-estimate of the lowest energy singlet transition energy.[31] Thus, the orbital labeled LUMO+1 should be considered the lowest unoccupied molecular orbital in the case of the Ln(III) complexes. As can be seen from Figure 2, the HOMO → LUMO+1 transition can be described as a π−π* transition for both systems. Importantly, the second lowest singlet energy (*i.e*. $S_0 \rightarrow S_2$) can be described as a combination of the HOMO → LUMO+2 and HOMO–1 → LUMO+1 transition and these evidently possess some intra ligand charge transfer (ILCT) character. For the **L^1** linkage, this ILCT is from the bridge to the central 1,2-HOPO chromophore while for **L^3**, the HOMO → LUMO+2 has significant ILCT character from the chromophore to the bridge.

As can also be seen in Tables 1 and 3, the estimated singlet ground state energies and the triplet excited state energies match well with the experimental data. In particular, the triplet excited state is predicted to be near 21,000 cm^{-1}, in agreement with the previous 1,2-HOPO derivatives already published[23-25] and is of an energy to efficiently sensitize the europium cation.

3. UV/visible absorption spectroscopy

The UV/visible absorption data for each of the Eu(III) and Gd(III) complexes in the different solvents are summarized in Table 2. Each of the spectra have absorption maxima around 335-340 nm which are composed of two electronic transitions; at lower energy a purely π−π* transition and a slightly higher energy (around *ca*. 320nm) π−π* transition with some CT character, as evidenced by the accompanying TD-DFT calculations (see Figure 2). The absorption maxima follow the expected trend, displaying a red shift with increasing conjugation, going from 336 nm to 342 nm in buffered aqueous solution for the **L^3** and **L^1** derivatives respectively. The molar absorption coefficients are within experimental error, with typical values around 20,000 $M^{-1}cm^{-1}$ which is also in agreement with previous results for the aliphatic bridged 1,2-HOPO derivatives.[24, 25] Thus, conjugation of a phenyl unit with the 1,2-HOPO chromophore through an amide function does not yield any relevant increase of the molar absorption coefficient. In methanol and DMSO, similar trends in the position of absorption maxima and the value of the molar absorption coefficients were observed.

No differences were observed when comparing the gadolinium and europium complexes, showing the absence of an effect due to the lanthanide cation in the ground state.

4. Luminescence properties of the gadolinium complexes

In order to estimate the energies of the ligand-based triplet excited state, the Gd(III) complexes were studied. Gadolinium is a $4f^7$ lanthanide cation with almost the same electronic structure and size as the europium cation ($4f^6$), but lacks an accessible metal-based low energy electronic excited state. For these complexes, at room temperature, only a broad weak emission centered around 400 nm can be seen for **$[Gd(L^2)_2]^-$** and **$[Gd(L^3)_2]^-$** while **$[Gd(L^1)_2]^-$** is almost not emissive (see Supporting Information Figure S1). This emission can be attributed to the singlet excited state of the 1,2-HOPO chromophore complexed to the gadolinium cation.

At 77K, in solid matrix, an emission band at *ca*. 500 nm can be seen. This emission, red shifted compared to the singlet excited state, is assigned to the triplet excited state below the singlet excited state observed at room temperature, as illustrated in Figure 4a where the luminescence spectra of the three gadolinium complexes at 77K are depicted. From these spectra, it appears the triplet excited states of the complexes are located at almost the same energy, varying from 496 nm to 504 nm for **$[Gd(L^2)_2]^-$** and **$[Gd(L^3)_2]^-$** respectively.

Moreover, this slight shift seems to arise as a result of the differing linewidths of the emission band rather than on any difference in the position of the maxima for the first vibronic transition (see Figure 4a). To confirm that the triplet excited is globally the same for the three complexes, spectral deconvolution of the triplet excited state emission ($T_{0\text{-}0}$) into a vibronic progression of several overlapping Gaussian functions with separations of *ca*. 1000-1100 cm^{-1} were performed[25, 32, 33] as presented on Figure 4.

After deconvolution, it was readily apparent that the triplet excited states have almost identical energies, ranging from 20,870 cm^{-1} to 21,230 cm^{-1} (Table 3). It is important to note that this energy is ideal for excitation of this ligand, which, as demonstrated elsewhere, efficiently sensitizes europium luminescence with overall quantum yields on the order of 20%.[24, 25]

Noticeably, since the triplet excited state energies of all these ligands are identical, no difference in the energy transfer efficiency is expected, and thus the observed differences in the excited singlet/triplet gap cannot be interpreted with confidence.

5. Luminescence properties of europium complexes

The emission spectra are typical for Eu(III) 1,2-HOPO derivatives, with very intense J = 2 transition ($^7F_2 \leftarrow {}^5D_0$) that represents around 84% of the total emission intensities (Figure 5). The spectra also look very similar in different solvents, the only changes observed are with the intensity of the J = 1 band ($^7F_1 \leftarrow {}^5D_0$) as compared to the overall intensity (Figure 5), yielding different radiative parameters (*vide infra*).

For the steady state emission spectra, the luminescence quantum yields and luminescence lifetimes of the Eu(III) complexes were also measured in three different solvents (aqueous with 0.1 M TRIS buffer pH= 7.4, methanol and DMSO solutions) in order to determine the relevant radiative and non-radiative parameters in these differing environments. Where possible, the luminescence lifetimes were also measured in the corresponding deuterated solvents, in order to estimate the number of bound solvent molecules in the inner sphere (*i.e.* *q* in water[34], and *n* in methanol[35]) using the empirical Horrocks equations.

The results presented in Table 3 and 4 show that the bridge has an important influence on all of the various photophysical parameters. For instance, the quantum yield of $\mathbf{[Eu(L^1)_2]^-}$ and $\mathbf{[Eu(L^3)_2]^-}$ are low compared to $\mathbf{[Eu(L^2)_2]^-}$ (6.2% and 5.1% *vs*. 23.1%, respectively) in buffered aqueous solution. Furthermore, the luminescence quantum yields in methanol are all higher than the values in water; the quantum yields range from 5% to 23% in buffered aqueous solution (with the best value for $\mathbf{[Eu(L^2)_2]^-}$) and corresponding values as high as 34.0% in methanol. The luminescence lifetimes are also significantly different from each other, which is attributed to the solvation of the complexes in the different media. Estimates of *q* reveal the presence of one molecule of water in the inner sphere for $\mathbf{[Eu(L^3)_2]^-}$ while, for the other complexes, there are no water molecules in close proximity to the metal. The same trend is observed in methanol, with values around 0.5 and 1.5. These values can be considered as slight overestimates, since the original Horrocks methanol equation does not account for the presence of second sphere solvent molecules nor the quenching effects of proximal N-H vibrations. Importantly, despite a small shift of the triplet excited state, the observed variations in quantum yield and also of luminescence lifetimes are significant, which would not be the case if the sensitization efficiency were only related to the energy of the triplet excited state. Moreover, the obvious luminescence quantum yield differences between $\mathbf{[Eu(L^1)_2]^-}$ and $\mathbf{[Eu(L^2)_2]^-}$ are not accompanied by relevant changes in their luminescence lifetimes. This confirms that, while the triplet excited state energies undoubtedly play an important role in the sensitization process differences, they are not the only critical factor. The geometry of the ligand around the Ln(III) ion induces different

intersystem crossing and energy transfer efficiencies to the Eu(III) cation that also are a crucial factor. The same conclusion can be drawn by comparing **$[Eu(L^3)_2]^-$** in non-protic medium to **$[Eu(L^2)_2]^-$** and **$[[Eu(L^1)_2]^-$**.

Luminescence lifetimes were also determined at 77K, in a solid matrix (Table 3), which allowed determination of whether back energy transfer between the donor triplet excited state and the acceptor manifold excited state of the lanthanide is present, or alternately whether quenching *via* low lying LMCT state occurs. In either case, luminescence lifetimes were found to be a few order of magnitude lower in solution than at 77K,[36-38]

As can be seen from Table 3 by comparing the 77K measurements to those in methanol solution, no such quenching occurs since there is only a small difference between the luminescence lifetimes in solution and in solid state (77K). Hence, we conclude that 1,2-HOPO derivatives possess a triplet state ideally located (around 20,000 and 21,000 cm^{-1}) for efficient energy transfer to the europium $^5D_1$ level.

6. Quantitative determination of the Eu^{III} sensitization parameters

Following the work of Beeby *et al*.[21] and of Verhoeven *et al*.[22], the efficiency of the sensitization can be estimated using a method that defines the overall quantum yield of luminescence (ϕ_{Eu}) as the product of the efficiency of the intersystem crossing (η_{ISC}), the efficiency of the energy transfer (η_{ET}) and the efficiency of metal centred luminescence (η_{Eu}).

$$\phi_{Eu}=\eta_{ISC}\,\eta_{ET}\,\eta_{Eu}=\eta_{sens}\,\eta_{Eu}$$

In this equation, the $\eta_{ISC}\,\eta_{ET}$ term cannot be easily broken into its individual components, and the product is instead termed the sensitization efficiency, η_{sens} ($\eta_{sens}=\eta_{ISC}\,\eta_{ET}$). The overall quantum yield of luminescence, ϕ_{Eu}, is determined experimentally while η_{Eu} is determined as:

$$\eta_{Eu}=\tau_{Eu}/\tau_R$$

where τ_{Eu} is the measured Eu lifetime and τ_R is the pure radiative lifetime that can be estimated from the emission spectra as follows:

$$k_R=1/\tau_R=A(0,1)[I_{tot}/I(0,1)]$$

The constant $A(0,1)$ is the spontaneous emission probability of the $^5D_0\rightarrow{}^7F_1$ transition, equal to 32.3 s^{-1} in water and $I_{tot}/I(0,1)$ is the ratio of the total integrated emission intensity to the intensity of the $^5D_0\rightarrow{}^7F_1$ transition.

The result of the k_R can be correlated to the variation of the sum of the non-radiative decay constant:

$$\sum k_{nr}=[(1/\tau_{Eu})k_R]$$

These parameters were calculated for the three complexes in the three different solvents and are reported in Table 4 for aqueous, methanolic and DMSO solutions respectively.

As can be seen from Table 4, there are close similarities among the parameter values for the best sensitizers **[Eu(L^2)$_2$]$^-$** and **[Eu(L^4)$_2$]$^-$** (previously reported[24, 25]). The slight increase in luminescence quantum yield of **[Eu(L^2)$_2$]$^-$** is due to the efficiency of the sensitization (53.0% *vs*. 48.5%), which leads to increased overall emission quantum yield for **[Eu(L^4)$_2$]$^-$**. For **[Eu(L^3)$_2$]$^-$**, all the parameters related to the europium center (τ_{Eu} and η_{Eu}) are very low because of the inner sphere water molecule bound to the metal cation, and hence the non-radiative decay rate is high (Σk_{nr}). Despite this, the sensitization process for **[Eu(L^3)$_2$]$^-$** is almost as good as that of **[Eu(L^2)$_2$]$^-$**. Finally, for **[Eu(L^1)$_2$]$^-$**, the low quantum yield in water can be attributed to an inefficient sensitization process (η_{sens}= 17.0%)[39] whereas the remaining parameters are only slightly lower than for **[Eu(L^2)$_2$]$^-$**, which has similar properties in terms of the efficiency of metal centered luminescence.

The analogous study in methanol also reveals that **[Eu(L^2)$_2$]$^-$** possesses optimized parameters for sensitization as in water yielding an overall 48.8% luminescence quantum yield, with an efficiency of sensitization close to 70%. Since methanol also possesses an OH group, the same problem for **[Eu(L^3)$_2$]$^-$** in aqueous solvent can be observed, namely a residual inner sphere solvent molecule leading to a high non-radiative decay rate constant. Nonetheless, the quantum yield is good (18.8%) considering the presence of a molecule of methanol in the inner sphere. Here again, the limiting factor is based on the metal's intrinsic luminescence properties. For **[Eu(L^1)$_2$]$^-$**, as in water, the sensitization efficiency is the limiting factor (16.2%). Notably, the luminescence quantum yield in methanol is higher for **[Eu(L^3)$_2$]$^-$** than for **[Eu(L^1)$_2$]$^-$** proving that the sensitization efficiency is more important that the presence of a solvent molecule in such solvent.

Lastly, since DMSO is a non protic solvent, this removes the effect of the OH vibration on the metal luminescence. As can be seen from Table 4, in DMSO, **[Eu(L^3)$_2$]$^-$** has an impressive luminescence quantum yield (31.9%) with an efficient sensitization process (60.3%) and a europium efficiency (45.7%) close to the one obtained for our best Eu complex. It is also worth pointing out the 100% efficiency of the sensitization process for **[Eu(L^2)$_2$]$^-$** in DMSO, which shows that the sensitization within the system is almost fully optimized, with a luminescence quantum yield of 47.6%. By contrast, for **[Eu(L^1)$_2$]$^-$**, the same problem of inefficient sensitization can be observed in DMSO, demonstrating that the bridge (and geometry change) in this case influences the sensitization process more than the metal related parameters.

Conclusion

In conclusion, the Eu(III) HOPO complexes are promising for time resolved luminescence application. In order to see the effect of geometry and electronic properties of the bridge on the optical properties, three complexes containing 1,2-HOPO derivatives bridged by aromatic units have been prepared and studied. The photophysical properties of the Gd(III) and Eu(III) complexes have been evaluated together with supporting TD-DFT calculations for the ligand in a model compound. Upon sensitization of the Eu(III) cation, these three systems behave quite differently for reasons which are not related to the triplet excited state energies. While one acts as an efficient europium sensitizer ((**L^2**), 23.1% luminescence quantum yield in 0.1 M TRIS aqueous solution), the two other systems give poor sensitization, for different reasons: for **[Eu(L^3)$_2$]$^-$**, the low quantum yield and luminescence lifetime are due to the presence of a water molecule bound in the inner sphere of the metal centre (*i.e*. low values of all parameters related to the europium centre), while for **[Eu(L^1)$_2$]$^-$**, the low emission quantum yield is mainly due to an inefficient sensitization process (*i.e*. intersystem crossing, energy transfer or both phenomena). To conclude, these three different complexes illustrate the effect of coordinated ligand geometry on the antenna properties that result in different sensitization and/or metal-centered luminescent properties.

The use of such bridge allows to obtain bright Eu(III) complexes (23.1%) but the geometry around the metal can also yield a poor sensitization efficiency. Work toward better understanding this sensitization process is currently in progress in our group.

Supplementary Material

Refer to Web version on PubMed Central for supplementary material.

Acknowledgments

This work was partially supported by the NIH (Grant HL69832) and supported by the Director, Office of Science, Office of Basic Energy Sciences, and the Division of Chemical Sciences, Geosciences, and Biosciences of the U.S. Department of Energy at LBNL under Contract No. DE-AC02-05CH11231.

References and notes

1. Handl HL, Gillies RJ. Life Sci. 2005; 77:361–371. [PubMed: 15894006]
2. Petoud S, Cohen SM, Bünzli J-CG, Raymond KN. J Am Chem Soc. 2003; 125:13324–13325. [PubMed: 14583005]
3. Song B, Wang G, Tan M, Yuan J. J Am Chem Soc. 2006; 128:13442–13450. [PubMed: 17031957]
4. Borisov SM, Wolbeis OS. Anal Chem. 2006; 78:5094–5101. [PubMed: 16841934]
5. Stich MI, Nagl S, Wolbeis OS, Henne U, Schaeferling M. Adv Funct Mater. 2008; 18:1399–1406.
6. Parker D. Coord Chem Rev. 2000; 205:109–130.
7. Tremblay MS, Halim M, Sames D. J Am Chem Soc. 2007; 129:7570–7577. [PubMed: 17518468]
8. Kido J, Okamoto Y. Chem Rev. 2002; 102:2357–2368. [PubMed: 12059271]
9. Kang T-S, Harrison BS, Foley TJ, Knefely AS, Boncella JM, Reynolds JR, Schanze KS. Adv Mater. 2003; 15(13):1093–1097.
10. De Bettencourt-Dias A. Dalton Trans. 2007:2229–2241. [PubMed: 17534483]
11. Kuriki K, Koike Y, Okamoto Y. Chem Rev. 2002; 102:2347–2356. [PubMed: 12059270]
12. Kim HK, Roh SG, Hong K-S, Ka J-W, Baek NS, Oh JB, Nah MK, Cha YH, Ko J. Macromol Res. 2003; 11(3):133–145.
13. Julian-Lopez B, Planelles-Arago J, Cordoncillo E, Viana B, Sanchez C. J Mater Chem. 2008; 18(1):23–40.
14. Weber JKR, Felten JJ, Cho B, Nordine PC. Nature. 1998; 393:769–771.
15. Slooff LH, Polman A, Klink SI, Hebbink GA, Grave L, van Veggel CJM, Reinhoudt DN, Hofstraat JW. Opt Mater. 2000; 14:101–107.
16. Slooff LH, Blaaderen AV, Polman A, Hebbink GA, Klink SI, van Veggel CJM, Reinhoudt DN, Hofstraat JW. J Appl Phys. 2002; 91:3955–3980.
17. Moynihan S, Van Deun R, Binnemans K, Krueger J, von Papen G, Kewell A, Crean G, Redmond G. Opt Mater. 2007; 29:1798–1808.
18. Escribano P, Julian-Lopez B, Planelles-Arago J, Cordoncillo E, Viana B, Sanchez C. J Mater Chem. 2008; 18:23–40.
19. Bünzli J-CG, Piguet C. Chem Soc Rev. 2005; 34:1048–1077. [PubMed: 16284671]
20. Bünzli J-CG. Acc Chem Res. 2006; 39:53–61. [PubMed: 16411740]
21. Beeby A, Bushby LM, Maffeo D, Williams JAG. J Chem Soc Dalton Trans. 2002:48–54.
22. Werts MHV, Jukes RTF, Verhoeven JW. Phys Chem Chem Phys. 2002; 4:1542–1548.
23. D'Aléo A, Xu J, Moore EG, Jocher CJ, Raymond KN. Inorg Chem. 2008; 47:6109–6111. [PubMed: 18553909]
24. Moore EG, Xu J, Jocher CJ, Werner EJ, Raymond KN. J Am Chem Soc. 2006; 128(33):10648–10649. [PubMed: 16910637]
25. Moore EG, Xu J, Jocher CJ, Castro-Rodriguez I, Raymond KN. Inorg Chem. 2008; 47:3105–3118. [PubMed: 18311915]

26. Kawahara S-I, Uchimaru T. Z Naturforsch B. 2000; 55:985–987.
27. Xu J, Durbin PW, Kullgren B, Ebbe SN, Uhlir LC, Raymond KN. J Med Chem. 2002; 45(18): 3963–3971. [PubMed: 12190318]
28. Frisch, MJ.; Trucks, GW.; Schlegel, HB.; Scuseria, GE.; Robb, MA.; Cheeseman, JR.; Montgomery, JJA.; Vreven, TKKN.; Burant, JC.; Millam, JM.; Iyengar, SS.; Tomasi, J.; Barone, V.; Mennucci, B.; Cossi, M.; Scalmani, G.; Rega, N.; Petersson, GA.; Nakatsuji, H.; Hada, M.; Ehara, M.; Toyota, K.; Fukuda, R.; Hasegawa, J.; Ishida, M.; Nakajima, T.; Honda, Y.; Kitao, O.; Nakai, H.; Klene, M.; Li, X.; Knox, JE.; Hratchian, HP.; Cross, JB.; Bakken, V.; Adamo, C.; Jaramillo, J.; Gomperts, R.; Stratmann, RE.; Yazyev, O.; Austin, AJ.; Cammi, R.; Pomelli, C.; Ochterski, JW.; Ayala, PY.; Morokuma, K.; Voth, GA.; Salvador, P.; Dannenberg, JJ.; Zakrzewski, VG.; Dapprich, S.; Daniels, AD.; Strain, MC.; Farkas, O.; Malick, DK.; Rabuck, AD.; Raghavachari, K.; Foresman, JB.; Ortiz, JV.; Cui, Q.; Baboul, AG.; Clifford, S.; Cioslowski, J.; Stefanov, BB.; Liu, G.; Liashenko, A.; Piskorz, P.; Komaromi, I.; Martin, RL.; Fox, DJ.; Keith, T.; Al-Laham, MA.; Peng, CY.; Nanayakkara, A.; Challacombe, M.; Gill, PMW.; Johnson, B.; Chen, W.; Wong, MW.; Gonzalez, C.; Pople, JA. Gaussian 03; Revision C.02. Gaussian Inc.; Wallingford CT: 2004.
29. Scarrow RC, Riley PE, Abu-Dari K, White DL, Raymond KN. Inorg Chem. 1985; 24(6):954–967.
30. Gutierrez F, Tedeschi C, Maron L, Daudey J-P, Azema J, Tisnès P, Picard C, Poteau R. J Mol Struct Theochem. 2005; 756:151–162.
31. Dreuw A, Head-Gordon M. J Am Chem Soc. 2004; 126:4007–4016. [PubMed: 15038755]
32. Jirsakova V, Reiss-Husson F, Agalidis I, Vrieze J, Hoff AJ. Biochim et Biophys Acta. 1995; 1231:313–322.
33. de Weerd FL, Palacios MA, Andrizhiyevskaya EG, Dekker JP, van Grandelle R. Biochemistry. 2002; 41:15224–15233. [PubMed: 12484760]
34. Supkowski RM, Horrocks WD. Inorg Chimi Acta. 2002; 340:44–48.
35. Holz RC, Chang CA, Horrocks WD. Inorg Chem. 1991; 30:3270–3275.
36. Zucchi G, Ferrand A-C, Scopelliti R, Bünzli J-CG. Inorg Chem. 2002; 41(9):2459–2465. [PubMed: 11978113]
37. Katagiri S, Hasegawa Y, Wada Y, Yanagida S. Chem Letters. 2004; 33(11):1438–1439.
38. Jocher CJ, Moore EG, Pierce JD, Raymond KN. Inorg Chem. 2008; 47(18):7951–7953. [PubMed: 18707093]
39. We determined that inefficient sensitization arises from the fast non-radiative decay from the singlet or triplet excited states rather than from oxygen quenching because luminescence properties were unchanged upon degassing the solutions.

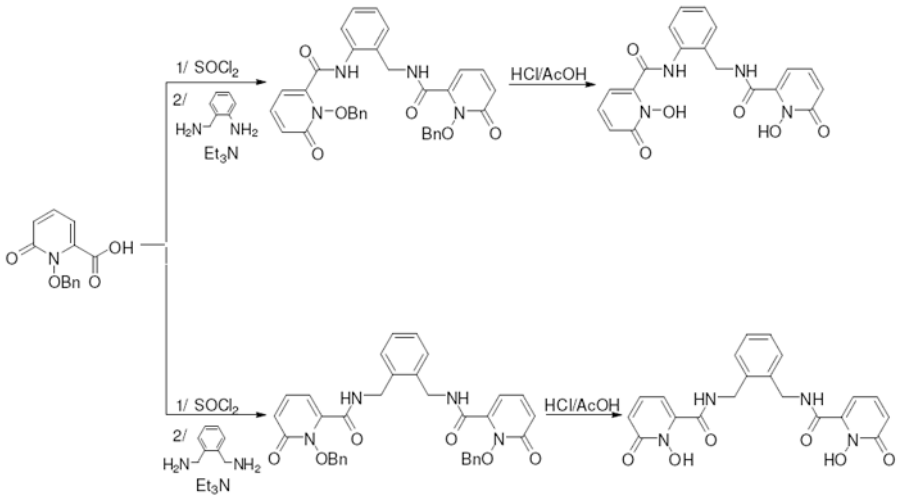

Figure 1.
Schematic representation of the synthesis pathway.

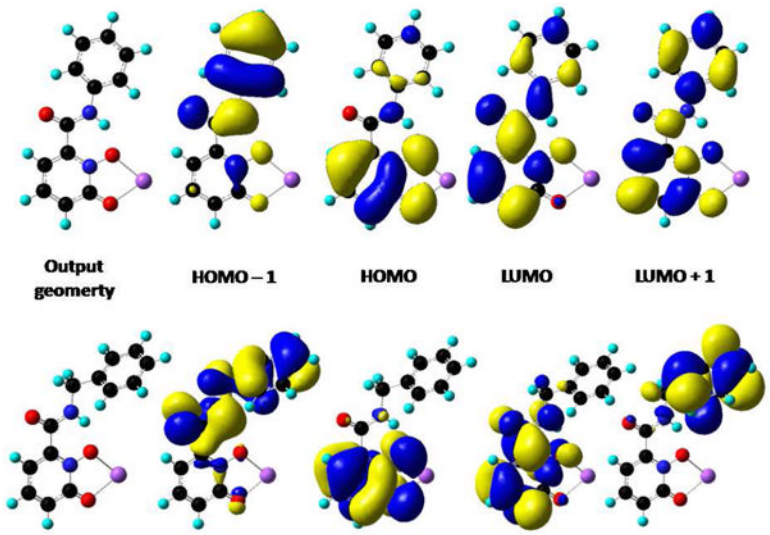

Figure 2.
Calculated output geometry obtained from static B3LYP/6-311G++ (d,p) geometry optimization and relevant corresponding molecular orbital diagrams from TD-DFT electronic structure calculations for a model **L^1Na** (top) and **L^3Na** (bottom) complexes.

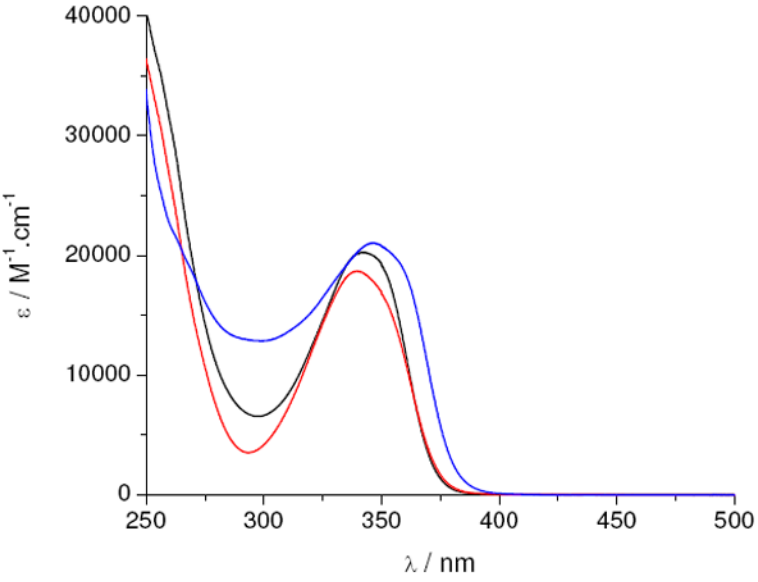

Figure 3.
UV/visible absorption spectra of **[Eu(L^1)$_2$]$^-$** (—) , **[Eu(L^2)$_2$]$^-$** (—) and **[Eu(L^3)$_2$]$^-$** (—) in 0.1 M TRIS buffered aqueous solution pH = 7.4.

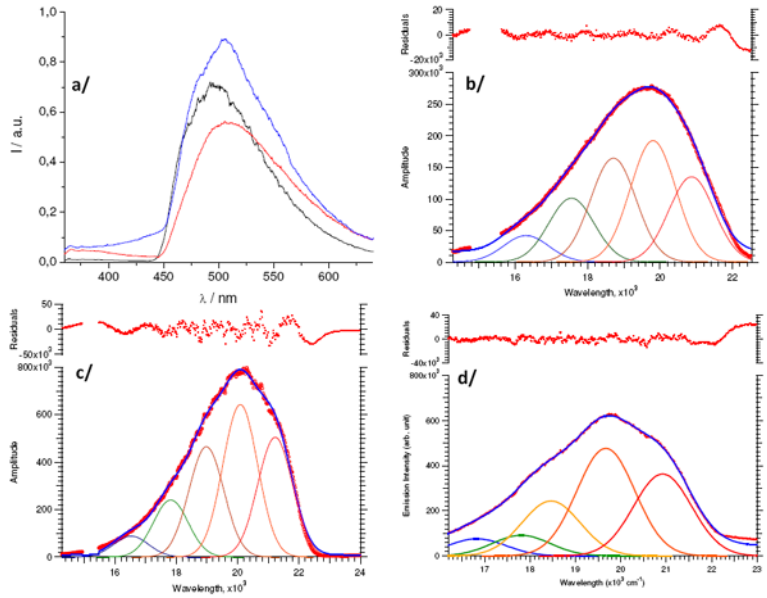

Figure 4.

Triplet excited state emission from Gadolinium complexes in solid matrix (77K, methanol/ethanol 1/4) (λ_{ex}= 320nm): a) $\mathbf{[Gd(L^1)_2]^-}$ (—), $\mathbf{[Gd(L^2)_2]^-}$ (—) and $\mathbf{[Gd(L^3)_2]^-}$ (—), b) deconvolution of $\mathbf{[Gd(L^3)_2]^-}$, c) deconvolution of $\mathbf{[Gd(L^2)_2]^-}$ and d) deconvolution of $\mathbf{[Gd(L^1)_2]^-}$.

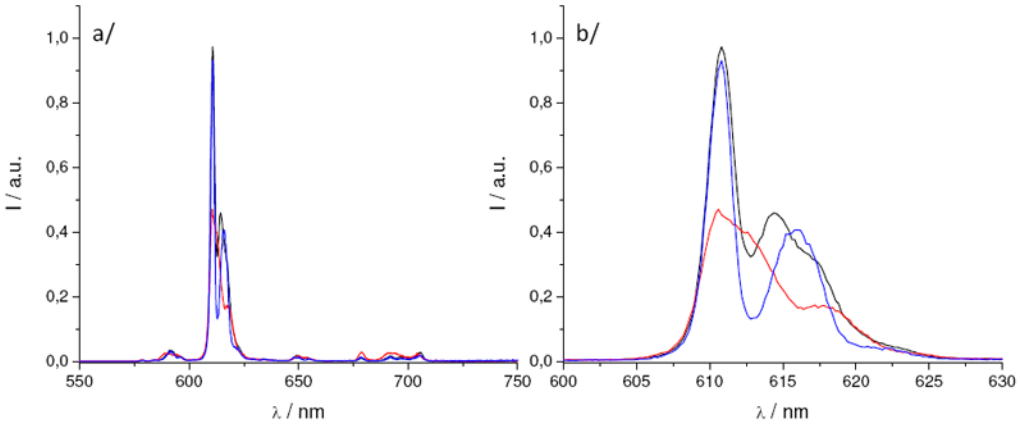

Figure 5.

Normalized luminescence spectra (on J= 1 transition) of $[Eu(L^1)_2]^-$ (—), $[Eu(L^2)_2]^-$ (—) and $[Eu(L^3)_2]^-$ (—) in aqueous TRIS solution (λ_{ex}= 340nm) a/ Full spectra, b/ J= 2 transition

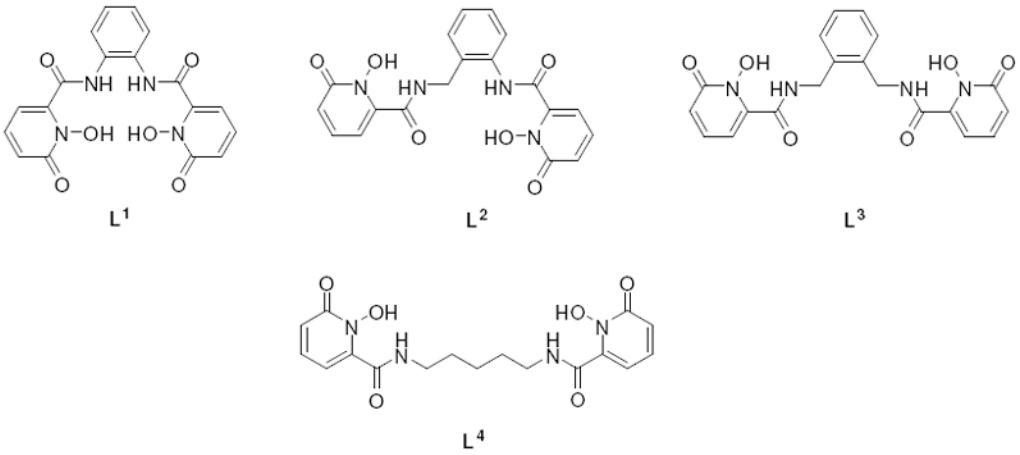

Chart 1.
Structures of the 1,2-HOPO ligands investigated.

Table 1

UV-visible absorption data of selected europium complexes in 0.1 M TRIS buffered aqueous solution (pH = 7.4) and corresponding data calculated for the model Na^+ complexes by TD-DFT.

	λ_{max} (nm)	ε^{max} ($M^{-1}cm^{-1}$)	λ_{max}^{calc} *a* (nm)	f *b*	λ_{max}^{calc} *c* (nm)	Assignment
$[Eu(L^1)_2]^-$	342	21,020	345.5	0.64	473.8	HOMO → LUMO + 1
$[Eu(L^3{}_2]^-$	337	18,690	333.5	0.64	483.2	HOMO → LUMO + 1

a wavelength of the lowest-energy singlet absorption band calculated by TD-DFT;

b calculated oscillator strength of the pertinent transition;

c wavelength of the lowest-energy triplet excited state calculated by TD-DFT.

Table 2

UV/visible absorption of the Eu(III) and Gd(III) complexes at room temperature in aqueous TRIS, methanol and DMSO solutions.

	Aqueous TRIS(pH 7.4)		Methanol		DMSO	
	λ_{abs} (nm)	ε ($M^{-1}cm^{-1}$)	λ_{abs} (nm)	ε ($M^{-1}cm^{-1}$)	λ_{abs} (nm)	ε ($M^{-1}cm^{-1}$)
$[Eu(L^1)_2]^-$	342[a]	21,020 [a]	345	21,780	346	20,140
$[Gd(L^1)_2]^-$	342 [a]	21,690 [a]	344	21,110	345	19,830
$[Eu(L^2)_2]^-$	338	20,260	343	21,220	342	20,430
$[Gd(L^2)_2]^-$	339	19,980	344	20,910	342	20,010
$[Eu(L^3)_2]^-$	337	18,690	340	20,640	343	19,980
$[Gd(L^3)_2]^-$	336	19,100	340	20,090	343	19,980

[a] sample containing 0.3% DMSO (volume).

Table 3

Photophysical data of the investigated complexes.

		Aqueous 0.1 M TRIS (pH= 7.4)				Methanol				DMSO		77K[c]
	T_{0-0}[b]	ϕ_{Eu}	τ (H) (µs)	τ (D) (µs)	q	ϕ_{Eu}	τ (H) (µs)	τ (D) (µs)	n	ϕ_{Eu}	τ (µs)	τ (µs)
$[Eu(L^1)_2]^-$	20,964	0.062[a]	536[a]	734[a]	0.2[a]	0.081	655	748	0.4	0.145	593	734
$[Eu(L^2)_2]^-$	21,230	0.231	567	766	0.1	0.340	623	736	0.5	0.476	740	662
$[Eu(L^3)_2]^-$	20,870	0.051	276	437	1.1	0.188	571	915	1.4	0.319	634	634

[a] sample containing 0.3% DMSO (volume),

[b] Determined using the Gd(III) complex at 77K in solid matrix (mixture of methanol and ethanol (1:4)),

[c] in solid matrix (mixture of methanol and ethanol (1:4)); H represents the hydrogenated solvent while D stand for the deuterated one.

Table 4

Photophysical data of the investigated complexes in water

Complex	Solvent	ϕ_{Eu}	ϕ_{Eu}^{theo}	τ_{Eu} / µs	τ_R / µs	η_{Eu}	η_{sens}	[I(0,1) / I_{tot}]	k_R / s^{-1}	Σk_{nr} / s^{-1}
$[Eu(L^1)_2]^-$	TRIS	0.062[a]	0.364[a]	536[a]	1470[a]	0.365[a]	0.170[a]	0.0475[a]	680[a]	1186[a]
	MeOH	0.081	0.500	655	1300	0.500	0.162	0.042	764	762
	DMSO	0.145	0.523	593	1134	0.523	0.277	0.050	882	804
$[Eu(L^2)_2]^-$	TRIS	0.231	0.436	567	1300	0.431	0.530	0.042	769	994
	MeOH	0.340	0.488	623	1276	0.488	0.696	0.052	784	821
	DMSO	0.476	0.462	740	1602	0.452	1.030	0.065	624	727
$[Eu(L^3)_2]^-$	TRIS	0.051	0.098	276	1680	0.164	0.522	0.054	595	5494
	MeOH	0.188	0.430	671	1618	0.415	0.430	0.041	618	818
	DMSO	0.319	0.529	634	1386	0.457	0.603	0.061	721	641
$[Eu(L^4)_2]^-$	TRIS	0.207	0.426	737	1728	0.426	0.485	0.056	579	778

[a] measured adding 0.3% DMSO (volume).